

THE MAGELLANIC BRIDGE: THE NEAREST PURELY TIDAL STELLAR POPULATION

JASON HARRIS

Steward Observatory and
933 North Cherry Ave., Tucson, AZ, 85721
Draft version July 14, 2018

ABSTRACT

We report on observations of the stellar populations in twelve fields spanning the region between the Magellanic Clouds, made with the Mosaic-II camera on the 4-meter telescope at the Cerro-Tololo Inter-American Observatory. The two main goals of the observations are to characterize the young stellar population (which presumably formed *in situ* in the Bridge and therefore represents the nearest stellar population formed from tidal debris), and to search for an older stellar component (which would have been stripped from either Cloud as stars, by the same tidal forces which formed the gaseous Bridge). We determine the star-formation history of the young inter-Cloud population, which provides a constraint on the timing of the gravitational interaction which formed the Bridge. We do not detect an older stellar population belonging to the Bridge in any of our fields, implying that the material that was stripped from the Clouds to form the Magellanic Bridge was very nearly a pure gas.

Subject headings: galaxies: evolution — galaxies: stellar content — galaxies: Magellanic Clouds — galaxies: interactions

1. INTRODUCTION

Interactions are known to be an important driver of galaxy evolution, but a detailed understanding of their influence remains elusive. The Magellanic Clouds are a particularly compelling target for investigating the effects of minor so-called “harassment” interactions, due to their proximity to the Milky Way, their close association over at least the past several Gyr, and their abundant gas reservoirs, which allow for ongoing star formation. The strongest evidence that their interaction has played an important role in driving the evolution of the Clouds lies in the extra-tidal features of the Magellanic Stream and Magellanic Bridge. Unlike the Magellanic Stream, which appears to be a pure-gas feature (Guhathakurta & Reitzel 1998), there is a known stellar population associated with the Magellanic Bridge, and by measuring the ages, chemical abundances, and kinematics of these stars, we can obtain strong constraints on the evolution of the dynamical event which formed the Bridge, and study in detail how star formation proceeds in the wake of such an event.

The Magellanic Bridge was first reported in H I observations by Hindman et al. (1963), and a young stellar component (the “inter-Cloud population”) was discovered by Irwin et al. (1985), who estimated the age of the stars at about 10^8 yr. Demers & Battinelli (1998) provided the most comprehensive study of the inter-Cloud population to date; they observed five fields in the western Bridge, and found stars as young as 10–25 Myr in both clusters and in a diffuse field component up to 9° from the SMC. The young inter-Cloud population probably formed *in situ* in the Bridge, in the wake of the Bridge-forming event, making it the nearest example of a stellar population whose formation was unambiguously triggered by a tidal interaction. Yet surprisingly, no detailed analysis of the star formation history of these stars has been performed to date, and we do not even know

the full extent of the population, since no fields along the ridgeline of the H I gas have been observed east of the midpoint between the Clouds.

Furthermore, no study to date has specifically searched for an older component of the inter-Cloud population, which would represent a population of stars that was stripped from the Clouds during the Bridge-forming event. Tidal forces during an interaction should affect both gas and stars, so the inter-Cloud population should have an old component, other things being equal.

The present study will address these open questions regarding the inter-Cloud population in the Magellanic Bridge. We present our observations and data reduction in Section 2. In Section 3.1, we trace the eastward extent of the young inter-Cloud population, and in Section 3.2, we search for tidally-stripped stars in our Bridge fields. We briefly examine the outer structure of the LMC using our four fields nearest that galaxy in Section 3.3. Finally, we present the star-formation history of the young inter-Cloud population in Section 3.4, and summarize the results in Section 4.

2. OBSERVATIONS AND DATA REDUCTION

2.1. *The Observations*

The data were obtained on the nights of January 4 and 5 2006 (UT), at the Cerro-Tololo Inter-American Observatory (CTIO) 4-meter telescope. We used the Mosaic-II camera, which images a $36' \times 36'$ field onto a $8k \times 8k$ CCD detector array, to obtain short and long exposures in Washington *C*, Harris *R*, and Cousins *I* filters at twelve field positions spanning the inter-Cloud region, and at one offset field at a similar Galactic latitude, but to the west of the SMC (see Table 1 and Figure 1).

The field positions were selected to uniformly sample the inter-Cloud region, approximately following the ridgeline of the H I gas which forms the Magellanic Bridge (Putman 2000). In addition, we selected two fields to lie off the main ridgeline, but still in regions of abundant H I emission (fields mb03 and mb14). Our

fields include the eastern half of the inter-Cloud region, where there are very few known star clusters, and where Demers & Battinelli’s fields mostly lie far from the H I ridgeline.

The exposure times listed in Table 1 were chosen in order to detect stars as faint as the ancient main-sequence turn-off with $S/N > 10$ in all three filters. At each field position and for each of the *C*, *R*, and *I* filters, we obtained a pair of long exposures for cosmic-ray rejection, and a short exposure to record the photometry of brighter stars that are saturated in the long exposures. Seeing was stable during both nights; the FWHM varied between $0.7''$ and $1.0''$. We observed standard star fields several times per night for photometric calibration (see Table 2), twilight flats were obtained during evening and morning twilight of both nights, and bias frames were obtained in the afternoon prior to both nights.

2.2. Data Reduction

The data reduction followed the procedure documented by the NOAO Deep Wide Field Survey team (Jannuzi et al. 2003), and utilized the `mscred` package in IRAF¹. Before reducing the data, we obtained an updated world coordinate system database for the CTIO 4-meter telescope from the CTIO website, dated from May 2004, and we also obtained an updated crosstalk-correction parameter file.

We first processed the bias frames using `ccdproc` and `zerocombine`. We then used `ccdproc` to perform overscan correction and trimming, bias subtraction, bad pixel masking, amplifier merging and crosstalk correction on all data images.

We ran `objmasks` on each twilight-sky exposure to mask out any detected stars in the images, and then combined the exposures using `sflatcombine`. This yielded normalized *C*, *R*, and *I* twilight-sky flats for each observing night. We then divided each data frame by the appropriate normalized flat, using `ccdproc` with the `sflatcor` parameter activated. To further flatten the data images, we also constructed night-sky flats from the collection of data images, after running `objmasks` on each image to mask out detected objects. We then ran `ccdproc` once again to apply the night-sky flats.

We empirically determined the world coordinate system (WCS) for each exposure using `mscmatch`, which uses an astrometric database to identify stars in the image and determine the WCS from their known coordinates. We chose to use the Guide Star Catalog, version 2 for the astrometric database, which we found yielded fit residuals that were smaller by about a factor of two compared to the USNO-A2 catalog. `mscmatch` provides an interactive interface with which the fit can be improved by eliminating outlying mismatched points. We were able to get the fit residuals in each image below 0.25 arcsec.

Next, we used `mscstack` to combine each pair of long exposures into a single, averaged image. We had initially activated the cosmic-ray rejection feature of `mscstack`,

but we found that if the seeing changed between the two exposures, the stellar flux in the averaged image would be significantly clipped by the rejection algorithm. Instead, we stacked the images without rejection, and used `craverage` to detect cosmic-ray hits in the combined image and replace the affected pixels with the average of the surrounding pixel values. We also ran `mscstack` on the short-exposure images, despite the fact that they did not have multiple exposures to combine, because `mscstack` also performs a pixel-value replacement for the pixels in the bad pixel masks.

The final step in the reduction pipeline is to run `mscpixarea`, which corrects each image for the variable pixel scale across the field. We then use `mscsplit` to separate the eight CCD images per field into separate FITS files. We choose to analyze the CCD images separately, in order to properly account for slight differences between the CCDs.

2.3. Instrumental Photometry

We used the `daophot` package in IRAF to perform stellar photometry on our images, using the method of point-spread function (PSF) fitting. For each CCD image, we ran `daofind` to identify peaks, and `phot` to obtain preliminary relative photometry of the detected sources.

Next, we used `pstselect` to select fifty bright, relatively isolated sources to form a high-quality sample from which an empirical PSF model will be built. Candidate PSF stars are rejected if they contain saturated pixels, or if their centers are within ten pixels of any pixel flagged as bad by our data reduction procedure.

The PSF fitting is performed in a fully automated way, without user intervention. However, we do examine residual images after PSF subtraction to ensure that the automatic model parameters are correct. All available forms for the PSF are explored to find the best-fitting model. Next, `group` and `nstar` are run to identify and photometer stars that are close neighbors of the PSF sample. `Substar` is used to subtract these close neighbors from the image. We then repeat the PSF fitting, this time using the neighbor-subtracted image to produce a more accurate model.

Once the second-pass PSF has been determined, we run `allstar` to perform iterative PSF photometry of all detected sources in the image. Then we run `daofind` on an image in which all known objects have been subtracted using the PSF model, in order to find fainter stars in the image. Then `allstar` is run on the subtracted image, using this new list of fainter stars². The two `allstar` photometry lists are combined into a single photometry table for the frame, and the IRAF task `wcsctran` is used to convert the stars’ X,Y pixel coordinates to right ascension and declination, using the world coordinate solution we determined during the data reduction procedure.

The above photometry procedure results in some spurious detections due to two artifacts: bleed columns, and scattered-light halos around extremely bright stars. The bleed columns are flagged as bad pixels by the data reduction procedure, but this does not prevent `daofind`

¹ IRAF is the Image Reduction and Analysis Facility, distributed by the National Optical Astronomy Observatories, which are operated by the Association of Universities for Research in Astronomy, Inc., under cooperative agreement with the National Science Foundation.

² Alternatively, we could have performed the second-pass `allstar` on the original image using a concatenated list of all detected objects. We tested both methods on an image from mb20, the most crowded field. The differences in the photometry are consistent with the uncertainties estimated by `allstar`

from identifying sources along the bleed columns, nor does it prevent `allstar` from trying to photometer these false sources. We therefore remove objects from the photometry table that are within 10 pixels of a flagged bad pixel. Extremely bright stars have large scattered-light halos in the images, resulting in circular concentrations of false detections centered on these stars due to the elevated flux levels. To clean the photometry tables of sources detected in the wings of extremely bright stars, we reject all sources with anomalously high estimated sky values. In the absence of these extremely bright stars, the sky levels are quite stable, making the sky levels an efficient way to identify spurious objects in the wings of bright objects.

The `allstar` program provides very accurate relative photometry, but because the PSF models are uncertain at large radii, the allstar magnitudes are normalized to a relatively small aperture size of 4 pixels. We therefore need to apply an aperture correction to convert the allstar magnitudes to true instrumental magnitudes that represent the total flux recorded from each star. To determine the aperture correction, we select bright, isolated objects from our sample and perform concentric-aperture photometry using `phot` with a series of aperture sizes, up to 17 pixels. The per-star aperture correction is simply the difference between the star’s allstar magnitude and its large-aperture magnitude: ($m_{als} - m_{ap17}$). However, since individual objects suffer from measurement errors and contamination from neighboring objects, we need to statistically determine the characteristic aperture correction for the entire frame. The distribution of per-star aperture-correction values is typically a Gaussian with an asymmetric tail to negative values. The Gaussian spread is due to measurement uncertainties, and the asymmetric tail is due to flux contamination, which is never completely mitigated by our selection of isolated objects.

An accurate determination of the aperture correction’s value and uncertainty requires that we attempt to isolate the underlying Gaussian shape from the asymmetric skew caused by contaminating flux. To do this, we first determine the approximate position of the distribution’s peak, and then fit a Gaussian function to the points to the positive side of this peak value, thereby ignoring the negative half that may suffer from flux contamination. We adopt the central value of the fitted Gaussian as the frame’s aperture correction, and its width as the uncertainty in the frame’s aperture correction. The instrumental magnitude of each star is simply its allstar magnitude plus the frame’s aperture correction; we also add the aperture correction uncertainty in quadrature to each star’s photometric uncertainty.

2.4. Standard Star Observations and Photometric Calibration

The final step in our determination of the stellar photometry is to place the instrumental magnitudes we have measured onto a standard photometric system, using standard-star observations. Standard star fields were imaged several times on both of the observing nights. One standard field (SA 101) was observed at two separate visits on each night in order to measure the effect of atmospheric extinction.

The standard star observations are presented in Table 2. We selected well-known standard fields, first mea-

sured by Landolt (1973), expanded for wide-field CCD instruments by Stetson (2000), and calibrated for the Washington C filter by Geisler (1996). The standard fields were reduced using the pipeline procedure described in Section 2.2. We then identified sources in each standard field with `daofind`, and performed concentric-aperture photometry on all sources with `phot` in IRAF’s `daophot` package.

We use the measured aperture photometry of the observed standard stars, together with their total photometry as published by Stetson (2000) and Geisler (1996), to solve the following photometric calibration equation for each filter and each CCD in the Mosaic-II array, and independently for the two nights of observing:

$$M = m + A + B * (R - I) - C * X$$

where M is the published total magnitude, m is the observed instrumental aperture magnitude, A is the photometric zeropoint, B is the color term, $R - I$ is the star’s true color, C is the atmospheric extinction term, and X is the airmass. Once we have determined A , B and C for each CCD and filter, we will be able to convert the observed photometry of any star to its total photometry, given its observed color and the airmass at which it was observed.

We first determine C , the atmospheric extinction term, by examining the photometry from SA 101, the standard field that was observed at different airmasses during each night. The C parameter is independent of the color term and zeropoint, so we simply need to fit a linear regression through the observed stars’ magnitudes as a function of the observed airmass. The slope of the linear regression is C , the atmospheric extinction term. Note that we need not restrict ourselves to the actual standard stars for this step; since we only need the relative photometry to determine the extinction term, all of the stars observed in field SA 101 can be employed.

Having determined C , we proceed to simultaneously determine the zeropoint and color term. The observed magnitudes of all standard stars are first corrected for atmospheric extinction ($m_x = m - C * X$); we then construct the quantity $M - m_x$, the difference between the the published total magnitude of the star and its extinction-corrected instrumental magnitude, and fit a linear regression through the $M - m_x$ values as a function of the published $R - I$ colors. The slope of this regression is the color term B , and its zeropoint is A , the photometric zeropoint correction. Table 3 presents the photometric calibration parameters for each CCD and filter, and for each of the two observing nights.

Note that in Table 3, the parameters for the Washington C filter are the same in all eight CCDs. The reason for this is that there are too few standard stars calibrated for the C filter to support an independent determination for each CCD (see Table 2), so we were forced to determine an average C calibration for the entire mosaic.

As noted in Table 3, there were too few R and I standards present in some of the CCDs to support an independent determination of their color terms and zeropoints. For these cases, we perform a bootstrap estimate of the parameter values from those published at the

CTIO website³. We determine the mean offset between our determined values of the photometric calibration parameters, and those published by CTIO, for the CCDs that we were able to analyze. We then apply this mean offset to the published values of the remaining CCDs, as an estimate of what we would have measured if we had observed enough standard stars in those CCDs. For the uncertainty in these bootstrapped parameters, we simply adopt the standard deviation of the mean offset between the observed and published values.

We simultaneously perform a positional match of the sources in the C , R and I photometry lists, and apply the above photometric calibration to produce catalogs with total CRI photometry. We then match objects between the CRI catalogs from the short and long exposures of each field. For the positional matching, we use a maximum match radius of $0.5''$; to be retained in the catalog, an object must be detected in the R band, with a matching detection in either C or I . For objects which are matched between the short and long exposures, we adopt the weighted mean photometry in the final catalog; objects present only in the short or long catalog are included as well. The final calibrated composite photometry catalogs for the twelve observed fields in the Magellanic Bridge (plus the observed offset field) are presented in Table 4, and rendered as pairs of Hess diagrams in Figure 2. A Hess diagram is a pixelized color-magnitude diagram (CMD) in which each pixel value is proportional to the number of stars in the region covered by that pixel. The CMD of the offset field is presented separately in Figure 3.

2.5. Statistical Subtraction of Foreground/Background Contamination

It is clear from comparing Figures 2 and 3 that the stellar populations in many of the fields are dominated by foreground Galactic (and background extragalactic) contamination. In order to study the underlying inter-Cloud populations, we need to first perform a statistical subtraction of the contaminant foreground/background population. In doing so, we will assume that the population observed in the offset field is representative of the contaminant population in each Bridge field (a reasonable assumption, given the similar Galactic latitude of the offset field).

We proceed by first determining a scaling factor for normalizing the number of objects in the offset field to the number of contaminant objects in each Bridge field. This is necessary to account for variations in the effective area covered by each field (which arise from masking out regions contaminated by bad pixels, very bright stars and bleed trails). The normalization factor is simply the ratio of object counts in the target and offset fields, for a selected subregion of each CMD that is expected to contain only contaminant objects. For the $C - R$ CMD, the normalization region is defined by the criteria $C - R > 2.4$, $R < 22.4 - (C - R)$, and $R > 23.8 - 2 * (C - R)$; for the $R - I$ CMD the criteria are $R - I > 1.0$ and $18 < I < 20$. The normalization regions are outlined with dashed lines in Figure 3. In the $C - R$ CMD, the objects in the normalization region constitute 12% of the total number of objects, while in the $R - I$ CMD, the fraction is 14%.

The normalization factor computed for each target field ranges between 0.65 and 0.95. We multiply the offset field's Hess diagrams by these scaling factors, and subtract them from the target field's Hess diagrams. The resultant statistically-cleaned Hess diagrams for each field are shown in Figure 4.

The statistical subtraction was generally successful in removing a component from each field's CMD that is consistent with the contaminant population in the offset field. However, there are some artifacts present that bear explanation. Specifically, the faint end of many of the $R - I$ CMDs appear to show an oversubtracted contaminant population. This is simply due to the fact that the offset field's $R - I$ CMD has a fainter detection limit than that in most of the target fields.

3. ANALYSIS

3.1. Extent of the Young Inter-Cloud Population

Young (age < 1 Gyr) stars provide an unambiguous tracer of the inter-Cloud population, because no foreground or background contaminants are expected to share the bright, blue region of the CMD with these stars. From previous work on the young inter-Cloud population by Demers & Battinelli (1998), we expected to observe a population of young stars near the SMC, coincident with the young cluster population cataloged by Bica & Schmitt (1995). However, we did not know how far the young population would extend toward the LMC along the H I ridgeline. We isolate stellar populations younger than 1 Gyr in the $C - R$ CMD, by selecting those stars with $R < 20$ mag and $C - R < 0$ mag (see dashed lines in Figure 2). Stars matching these criteria are absent in all of our fields east of mb09, which corresponds roughly to the eastern extent of the Bica & Schmitt clusters. Interestingly, field mb09 is also near the position along the H I Bridge where the gas surface density drops to the critical threshold for star formation of $3-4 M_{\odot} pc^{-2}$ (Kennicutt 1989), which corresponds to the $5 \times 10^{21} cm^{-2}$ seen throughout the eastern Bridge in Figure 4a of Brüns et al. (2005). West of field mb09, the gas density is sustained at a level three times higher, and this is where star formation has been active in the Bridge. It would seem that the same star formation threshold observed for disk galaxies holds for this tidal debris environment as well.

3.2. Searching for Tidally-Stripped Stars in the Inter-Cloud Region

It is perhaps not surprising that the young inter-Cloud population is confined to those regions where the gas density is relatively high, if we accept the hypothesis that these stars formed *in situ*, following the formation of the gaseous Bridge by a recent gravitational encounter between the Clouds. However, the tidal forces that presumably formed the Bridge should have stripped stars and gas with equal efficiency, so we expect to observe a population of such tidally-stripped stars in the inter-Cloud region. Yoshizawa & Noguchi (2003) conducted detailed numerical modeling of the stars and gas in the SMC, as it orbits both the LMC and Milky Way, in an attempt to reproduce the broad physical parameters of the Magellanic system. In their best-fitting model, there is an abundant population of stars in the inter-Cloud region which formed in the SMC, and had been ejected

³ <http://www.ctio.noao.edu/mosaic/ZeroPoints.html>

into the inter-Cloud region by a tidal interaction with the LMC. The tidally-stripped stars should have a similar age distribution to the stars in the galaxy from which they were stripped (at least for ages prior to the Bridge-forming event when their histories diverged). Since the stellar populations in both Magellanic Clouds exhibit a prominent red giant branch and a “red clump” horizontal branch, these bright features serve as ideal tracers of a putative stellar population that had been stripped from either of the Clouds during the Bridge-forming event.

While some of the fields in Figure 4 do show red giant branch and red clump features, these older populations appear to be confined to the fields nearest the SMC (fields mb02 and mb03) or the LMC (fields mb16–mb20). Furthermore, the surface density of these tracer populations increases sharply as the galactocentric separation of the field decreases, consistent with populations that are bound to the LMC and SMC. In Section 3.3, we will demonstrate that the red giant populations in fields mb16–mb20 are consistent with a plausible exponential disk distribution centered on the LMC. For now, we simply conclude that the red giant populations in these six fields near the SMC and LMC are very likely composed of stars bound to each respective galaxy, and are not indicative of a tidally-stripped stellar population in the Magellanic Bridge.

The Hess diagrams of the remaining six fields (mb06–mb14) show no red features that can be associated with an old inter-Cloud population. However, the strength of this non-detection is limited by the presence of the contaminant population. To enhance our sensitivity to a potentially sparse old stellar population, we construct a composite pair of Hess diagrams from these six “true Bridge” fields, and perform a new statistical contaminant subtraction on the composite population (see left panels of Figure 5). Even in this composite Hess diagram which covers more than two square degrees of the inter-Cloud region, there is no detectable trace of an underlying red giant branch or red clump feature.

We can place an upper limit on the surface density of red giant branch stars in these six “true Bridge” by adding an artificial old stellar population at the distance of the Magellanic system ($m - M = 18.7$ mag, intermediate between the two Clouds) to the composite inter-Cloud population. The artificial old stellar population is drawn from a theoretical isochrone (Girardi et al. 2002) with $Z = 0.002$ and $\log(\text{age}) = 10.0$, to which we add photometric errors consistent with the data. We modulate the number of artificial stars added until a red giant branch is marginally detectable (Figure 5). We conclude from this exercise that there are fewer than 1000 red giant branch stars at the distance of the Bridge and brighter than $R = 23$ mag in the observed composite population. By applying a stellar mass function (Kroupa 2001), we can convert the upper limit on the number of observed red giants to an upper limit on the total stellar mass present in a putative old stellar population. However, the conversion factor depends on the assumed age of the stars, because the fraction of the total stellar population that is brighter than $R = 23$ mag varies with age. For a 10 Gyr population, the upper mass limit is $14800 M_{\odot}$, and for a 2.5 Gyr population, the upper mass limit is $5300 M_{\odot}$. Thus, the stellar surface mass density in these six “true Bridge” fields is $\leq 0.009 M_{\odot} pc^{-2}$; this is more

than 400 times smaller than the average surface mass density of H I in the Magellanic Bridge ($4 M_{\odot} pc^{-2}$, converted from the characteristic column density in the Bridge, Brüns et al. 2005). There does not appear to be any trace of a tidally-stripped stellar population in the Magellanic Bridge, at least in these six fields along the H I ridgeline.

One potential caveat in this analysis is that we have assumed that the putative tidally stripped stellar population would be spatially coincident with the gaseous Bridge. This need not be the case; if ram-pressure from the Milky Way halo has played a significant role in the evolution of the Magellanic system (Mastropietro et al. 2005), then it is possible that the gaseous Bridge is now displaced from the region occupied by tidally-stripped stars between the Clouds. We investigate this possibility using data from the 2-Micron All-Sky Survey (2MASS, Skrutskie et al. 2006).

Using the Gator web-based database query service⁴ at the NASA/IPAC Infrared Science Archive, we obtained near-infrared JHK photometry from the 2MASS All-Sky Point Source Catalog, in two regions (shown as dashed boxes in Figure 1). The first 2MASS region (the “full-bridge region”) was selected to cover all plausible locations where a tidally-stripped inter-Cloud population might exist. We selected a range in right ascension between 2.5^h and 3.5^h , because these limits are bracketed by fields mb06 and mb14, which define the edges of the “pure bridge” section of our sample, uncontaminated by LMC or SMC stars. We selected a very large range in declination, from -77° to -69° , to cover all plausible trajectories of a putative tidally-stripped stellar population. The second 2MASS region (the “SW-LMC region”) was selected as a comparison field that is known to contain an old stellar population at the distance of the Magellanic system. This region spans 4.2^h to 5^h in right ascension, and -75° to -74° in declination. It is coincident with our fields mb18, mb19 and mb20, in which we have observed an old stellar population associated with the LMC (Section 3.2). While the full-bridge region covers a solid angle ten times larger than that of the SW-LMC region (35 square degrees and 3.2 square degrees, respectively), the 2MASS catalog contains about the same number of stars in both regions (94000 stars in the full-bridge region, and 92000 stars in the SW-LMC region), due to the larger stellar surface density of the SW-LMC region.

The 2MASS $J - K$ CMDs for these two regions are shown in Figure 6. In the SW-LMC region, there is an abundant population of red objects consisting of old stars associated with the the LMC. Following Nikolaev & Weinberg (2000), we identify the various sub-populations of these red objects. The bulk of the population extends in a narrow diagonal sequence from $J - K = 1$ mag, $K = 14$ mag to $J - K = 1.25$ mag, $K = 11$ mag. Along this sequence, there is a sharp drop in the density of stars around $K = 12.3$ mag; this is the tip of the red giant branch. The stars in this sequence brighter than $K = 12.3$ mag are oxygen-rich asymptotic giants, while the stars which extend redward of $J - K = 1.25$ mag are carbon-rich asymptotic giants. In the full-bridge region’s $J - K$ CMD, there is a small number of stars whose photometry is consistent with these features (notably the ~ 6

⁴ <http://irsa.ipac.caltech.edu/applications/Gator>

red objects around $K = 11$ mag which may be Carbon stars at the Magellanic distance), but considering the very large solid angle covered by the full-bridge region, we do not regard these objects as a significant detection of an old inter-Cloud population. We can place an upper limit on the number of red giants at the distance of the Magellanic system that can remain undetected in the 2MASS CMD, using the same synthetic population analysis described above for our optical CMDs. A red giant population containing 150 stars brighter than $K = 14$ mag is easily detectable when added to the 2MASS CMD, which implies that any old inter-Cloud stellar population that may be present has a total stellar mass no greater than $2 \times 10^6 M_{\odot}$. This is 1% of the total H I mass in the Magellanic Bridge (Brüns et al. 2005). However, the area covered by our full-Bridge region is about three times smaller than the area used to define the Bridge by Brüns et al., so the true limit from the 2MASS data is closer to 3%. Thus, even accounting for the possibility that a putative tidally-stripped stellar population may be displaced from the gaseous Magellanic Bridge, we can still conclude that the Bridge material was more than 97% gas when the Bridge was formed.

3.3. The Outer Disk of the Large Magellanic Cloud

In fields mb16–mb20 we observe old stellar populations that we conclude are bound members of the LMC, based on the sharp increase in their surface density with decreasing angular separation from the LMC. Gallart et al. (2004) and others have found that the LMC’s stellar radial profile follows an exponential disk to projected radii beyond 7 kpc, with no sign of a break which might indicate the onset of a kinematic halo. Fields mb16–mb20 have projected separations from the LMC of between 5 kpc and 8.5 kpc; however, when the orientation of the LMC disk (van der Marel & Cioni 2001) is taken into account, the in-disk galactocentric distances of these fields are between 6 kpc and 10.5 kpc. We use the number of stars in the red clump feature as a proxy for the stellar surface density, and plot the surface density profile in Figure 7. The solid curve represents the best-fit exponential-disk model, with a scale length of $\alpha = 0.98$ kpc, and the dotted and dashed curves are exponential disk models fit by previous authors, as noted in the figure caption. The surface density profile of the red clump stars in fields mb16–mb20 are generally consistent with previous measurements of the LMC’s outer exponential disk, but the fact that the profile is somewhat steeper in this southwestern quadrant is interesting. A comprehensive survey of the stellar populations in the outer LMC is currently underway; we will therefore postpone further discussion of the LMC’s structure until this survey is completed, when more definitive conclusions can be made.

3.4. Characterizing the Purely Tidal Stellar Population in the Inter-Cloud Region

We have determined that the stars in the inter-Cloud region appear to be exclusively composed of a stellar population that formed *in situ*, in the wake of the Bridge-forming event (modulo some contribution from stars still bound to the LMC and to the SMC, in the observed Bridge fields nearest those galaxies). This isolation of

a tidally-triggered stellar population provides an important opportunity to examine the nature and evolution of star formation processes in tidal debris. We measure the age distribution of the inter-Cloud population to determine when the star formation occurred, and how long it lasted. Since these stars presumably formed in the wake of the Bridge-forming event, these measurements provide an important constraint on the timing of that event. We will also look for spatial structure in the age distribution, which may provide insights into how star formation proceeds when triggered by a gravitational interaction.

Previous studies of the inter-Cloud population have estimated the age of the youngest stars present, through simple isochrone fitting (e.g., Demers & Battinelli 1998). Here we will perform a more detailed analysis, using the StarFISH star formation history fitter (Harris & Zaritsky 2001). This analysis is motivated by the clear presence of composite stellar populations in some of our fields, and by our goal to constrain the duration of star-formation activity in the Bridge.

StarFISH constructs a library of synthetic CMDs, each of which represents a model of what the photometric observations would yield, if the observed stellar population had a single age and a single metallicity. The model photometry is derived from theoretical isochrones; in this case we chose the latest Padua isochrones (Girardi et al. 2002). In order to accurately predict the observed photometric distribution in the CMDs, the models include a distance modulus, a distribution of extinction values, and a detailed model of the photometric errors. The distance modulus was simply chosen to be that of the SMC, 18.9 mag, because the young stellar populations in the Bridge are near the SMC on the sky. The distribution of extinction values is drawn from regions near the eastern edge of the MCPS SMC extinction map (Zaritsky et al. 2002). For the photometric errors, we employ an analytic model that reproduces the error statistics in the observed fields. While we usually advocate for an empirical model based on artificial stars tests, these tests are only strictly necessary when the data images are crowded. In the present case, even in our field with the highest stellar surface density (mb20), we have detected roughly 109000 stars in 8192^2 pixels, corresponding to a mean separation between objects of almost 14 pixels.

The StarFISH model library provides synthetic CMDs for the range of ages and metallicities thought to be present in the observed population; in the present case we constructed synthetic CMDs for 16 age bins spanning ages 10 Myr to 12 Gyr, spaced uniformly in $\log(\text{age})$, and for three metallicity bins, $Z = 0.001$, $Z = 0.002$, and $Z = 0.004$. The best-fit SFH is found by determining the combination of amplitudes modulating these synthetic CMDs which produces a composite model CMD that most closely matches the observed CMD. To take advantage of the full *CRI* photometric data set in determining the SFH, the fit is actually performed on the CMD pair: $C - R$ vs. R and $R - I$ vs. I .

Because the contaminant population dominates many of our observed fields, it is important to account for contaminants in the SFH fit. We could have run StarFISH on the statistically-cleaned data set, but we instead chose to use the observed data set, and simply include the contaminant offset-field population as an additional ampli-

tude in the model, in addition to the normal set of synthetic CMDs. The code will then select a multiplicative amplitude factor that optimally accounts for the contaminant population, just as it does for each of the synthetic CMDs.

The star formation histories of our twelve observed Magellanic Bridge fields are presented in Figure 8, and the results are consistent with the qualitative analysis of the CMDs presented in Sections 3.1 and 3.2. Recent star formation has occurred only in the fields west of mb11, and old stellar populations are confined to the six fields nearest the SMC (mb02 and mb03) and LMC (mb16–mb20). In fields mb11, mb13 and mb14 there is no trace of a stellar population associated with the Magellanic system.

Our StarFISH analysis shows that star formation in the Bridge began around 200–300 Myr ago, and this measurement provides an important constraint on the timing of the Bridge-forming event. In field mb02, the field nearest the SMC, we see a prolonged star formation episode spanning ages 80–300 Myr, and in mb03 we see a slightly shorter episode spanning ages 100–200 Myr. In the other fields in which a young stellar population is present (mb06–mb09), the star formation rates are much lower, making ages and durations more difficult to determine reliably. To boost the signal, we construct a composite population from these three fields, and determine the SFH of the composite population (see Figure 9). In these more easterly fields, we see evidence for two distinct episodes of star formation, 160 Myr and 40 Myr ago. It is interesting that while star formation was active throughout the western Bridge 100–200 Myr ago, the more recent episode 40 Myr ago was apparently confined to regions further from the SMC. We note that Demers & Battinelli (1998) also found that the youngest inter-Cloud populations are to be found in fields eastward of the SMC Wing.

The StarFISH solutions indicate that no significant star formation occurred in the Bridge more recently than 40 Myr ago. This conclusion can be confirmed by direct inspection of the CMDs in Figure 2: in no region do we see a significant number of main sequence stars brighter than $R = 15$ mag, corresponding to the main-sequence turn off position of a 40 Myr isochrone at the distance of the Magellanic system.

The conclusion that star formation in the Bridge largely ceased around 40 Myr seems to be at odds with a variety of previous research that finds evidence of stellar populations much younger than this. Demers & Battinelli (1998) used main-sequence isochrone fitting to conclude that the western Bridge contains stars as young as 10–25 Myr. Meaburn (1986) reported the discovery of DEM 171, a large circular $H\alpha$ filament in the Bridge which is likely photoionized by one or more massive O stars. Bica & Schmitt (1995) found that some of the clusters in their Bridge catalog have associated emission nebulae, again implying the presence of massive stars. Mizuno et al. (2006) detected cold molecular clouds in the Bridge, which demonstrates at least the potential for ongoing star formation.

This apparent contradiction can be partly reconciled by understanding that we are not claiming there are absolutely no stars in the Bridge younger than 40 Myr; we find that the star-formation rate dropped off around 40 Myr ago, and has remained consistent with zero since

then. We also note that our field selection covers the HI ridgeline of the Magellanic Bridge uniformly (see Figure 1), *except* for the segment around $RA = 2^h$, where much of the evidence for more recent star formation is to be found. These explanations do not reconcile our result with the conclusions of Demers & Battinelli (1998), however. They reported the widespread presence of stars aged 10–25 Myr in a number of fields east of $RA = 2^h$. This is based on an analysis of their Figure 7 (lower panel), in which theoretical isochrones are overplotted on a composite CMD from four of their observed fields. While the observed main sequence does appear to follow the shape of the 10 Myr isochrone, it is clearly truncated around $M_V = -3$ mag, whereas a 10 Myr population should have a main sequence that extends up to $M_V = -5$ mag. A main sequence turn-off at $M_V = -3$ mag is consistent with the 40 Myr age that we have found for the youngest bulk population in the Bridge.

4. SUMMARY

We have observed stellar populations in twelve fields uniformly spanning the region between the Magellanic Clouds. Our fields were selected to follow the ridgeline of the H I gas that forms the Magellanic Bridge, in order to look for stars that formed *in situ* in the Bridge from gas that had already been removed from one of the Clouds, and also for stars that were stripped from either of the Clouds by the same tidal forces that presumably stripped the gas.

We observed the previously known young stellar population in the western half of the inter-Cloud region, most recently characterized by Demers & Battinelli (1998), and extend on previous analyses in two key ways. First, we determine that the eastward extent of these stars is truncated around $\alpha = 3^h$, corresponding also to the eastward extent of the star clusters cataloged by Bica & Schmitt (1995), and to the point at which the H I surface density falls below the critical threshold for star formation as determined by Kennicutt (1989). Second, we use the StarFISH program to determine quantitative star formation histories of the young inter-Cloud population, finding that star formation in the Bridge commenced about 200–300 Myr ago, and continued over an extended interval, until about 40 Myr ago.

We found no evidence for a population of tidally-stripped stars in the inter-Cloud region, and our non-detection allows us to conclude that the material stripped from the Clouds into the Bridge was very nearly a pure gas, with an upper limit on the mass fraction in stars of less than 10^{-4} if coincidence with the gaseous Bridge is assumed, and 0.03 otherwise. This can potentially be understood if the pre-collision SMC had an extended envelope of gas, surrounding a more tightly bound stellar component. In this case, a weak tidal interaction might unbind the gas envelope while leaving the stellar component undisturbed. It is known that some dwarf galaxies have H I gas extending beyond 2–3 times the radii occupied by their stellar populations (Salpeter & Hoffman 1996), so perhaps this scenario is plausible. In fact, the recent numerical simulation of the tidal history of the SMC by citeyn03 included such an extended gas envelope, in order to produce a pure-gas Magellanic Stream. Nevertheless, the inter-Cloud region in their

best model contains an abundant population of tidally-stripped stars. In addition, Figure 4a of Brüns et al. (2005) shows that the H I gas in the Magellanic Bridge appears to be contiguous with the higher-density gas in the central regions of the SMC, which are currently abundantly populated with stars. If the gaseous Bridge formed via the tidal extraction of this high-density gas from the central regions of the SMC, then the question remains: where are the stars in the Bridge that should have felt these same tidal forces?

Future observations may be able to address this question. While some kinematic measurements exist for a handful of stars in the inter-Cloud region (Maurice et al. 1987; Kunkel et al. 1997), radial-velocity kinematics of a truly representative sample of the young inter-Cloud population would help us to better understand the dynamical evolution of the Magellanic Bridge. A much deeper understanding of the SMC's complex three-dimensional structure and kinematics would certainly help as well. These measurements (along with our current understanding of the orbital motions of the Clouds and the Milky Way) could then be used to motivate new

detailed numerical simulations specifically targeting the formation of the Magellanic Bridge as a pure-gas feature. We may then better understand how tidal features are formed during minor harassment interactions, and what role such interactions play in driving the evolution of the participant galaxies.

I am very grateful for extended discussions with Edward Olszewski on the interpretation of the data presented here, and I would also like to thank Kurtis Williams, Abhijit Saha, Knut Olsen, Tim Abbot and Armin Rest for their assistance with the reduction of the Mosaic-II images. Finally, I would like to gratefully acknowledge the constructive comments made by the anonymous referee. These comments prompted the 2MASS analysis, and substantially improved the paper. JH is supported by NASA through Hubble Fellowship grant HF-01160.01-A awarded by the Space Telescope Science Institute, which is operated by the Association of Universities for Research in Astronomy, Inc., under NASA contract NAS 5-26555.

REFERENCES

- Bica, E. L. D. & Schmitt, H. R. 1995, *ApJS*, 101, 41
 Brüns, C., Kerp, J., Staveley-Smith, L., Mebold, U., Putman, M. E., Haynes, R. F., Kalberla, P. M. W., Müller, E., & Filipovic, M. D. 2005, *A&A*, 432, 45
 Demers, S. & Battinelli, P. 1998, *AJ*, 115, 154
 Gallart, C., Stetson, P. B., Hardy, E., Pont, F., & Zinn, R. 2004, *ApJ*, 614, L109
 Geisler, D. 1996, *AJ*, 111, 480
 Girardi, L., Bertelli, G., Bressan, A., Chiosi, C., Groenewegen, M. A. T., Marigo, P., Salasnich, B., & Weiss, A. 2002, *A&A*, 391, 195
 Guhathakurta, P. & Reitzel, D. B. 1998, in *ASP Conf. Ser.* 136: *Galactic Halos*, ed. D. Zaritsky, 22–+
 Hardy, E. 1978, *PASP*, 90, 132
 Harris, J. & Zaritsky, D. 2001, *ApJS*, 136, 25
 Hindman, J. V., Kerr, F. J., & McGee, R. X. 1963, *Australian Journal of Physics*, 16, 570
 Irwin, M. J., Kunkel, W. E., & Demers, S. 1985, *Nature*, 318, 160
 Jannuzi, B. T., Claver, J., & Valdes, F. 2003, *The NOAO Deep Wide-Field Survey MOSAIC Data Reductions*, <http://www.noao.edu/noao/naodeep/ReductionOpt/frames.html>
 Kennicutt, Jr., R. C. 1989, *ApJ*, 344, 685
 Kroupa, P. 2001, *MNRAS*, 322, 231
 Kunkel, W. E., Irwin, M. J., & Demers, S. 1997, *A&AS*, 122, 463
 Landolt, A. U. 1973, *AJ*, 78, 959
 Mastrogiuseppe, C., Moore, B., Mayer, L., Wadsley, J., & Stadel, J. 2005, *MNRAS*, 363, 509
 Maurice, E., Andersen, J., Ardeberg, A., Bardin, C., Imbert, M., Lindgren, H., Martin, M., Mayor, M., Nordstrom, B., Prevot, L., Rebeiro, E., & Rousseau, J. 1987, *A&AS*, 67, 423
 Meaburn, J. 1986, *MNRAS*, 223, 317
 Mizuno, N., Müller, E., Maeda, H., Kawamura, A., Minamidani, T., Onishi, T., Mizuno, A., & Fukui, Y. 2006, *ApJ*, 643, L107
 Nikolaev, S. & Weinberg, M. D. 2000, *ApJ*, 542, 804
 Putman, M. E. 2000, *Publications of the Astronomical Society of Australia*, 17, 1
 Salpeter, E. E. & Hoffman, G. L. 1996, *ApJ*, 465, 595
 Skrutskie, M. F., Cutri, R. M., Stiening, R., Weinberg, M. D., Schneider, S., Carpenter, J. M., Beichman, C., Capps, R., Chester, T., Elias, J., Huchra, J., Liebert, J., Lonsdale, C., Monet, D. G., Price, S., Seitzer, P., Jarrett, T., Kirkpatrick, J. D., Gizis, J. E., Howard, E., Evans, T., Fowler, J., Fullmer, L., Hurt, R., Light, R., Kopan, E. L., Marsh, K. A., McCallon, H. L., Tam, R., Van Dyk, S., & Wheelock, S. 2006, *AJ*, 131, 1163
 Stetson, P. B. 2000, *PASP*, 112, 925
 van der Marel, R. P. & Cioni, M.-R. L. 2001, *AJ*, 122, 1807
 Yoshizawa, A. M. & Noguchi, M. 2003, *MNRAS*, 339, 1135
 Zaritsky, D., Harris, J., Thompson, I. B., & Grebel, E. K. 2004, *AJ*, 128, 1606
 Zaritsky, D., Harris, J., Thompson, I. B., Grebel, E. K., & Massey, P. 2002, *AJ*, 123, 855

TABLE 1
 MOSAIC-II FIELDS AND EXPOSURES

Field ID	Right ascension	Declination	Filter	t_{exp} [sec]	Observing time [UT]	Airmass
Offset	00 ^h 13 ^m	-79° 59'	C	600	2006-01-04 01:19	1.68
...	R	300	2006-01-04 01:42	1.72
...	I	300	2006-01-04 01:56	1.74
...	C	20	2006-01-05 01:09	1.67
...	R	10	2006-01-05 01:11	1.68
...	I	10	2006-01-05 01:13	1.68
mb02	01 ^h 48 ^m	-74° 30'	C	600	2006-01-04 02:11	1.50
...	R	300	2006-01-04 02:34	1.54
...	I	300	2006-01-04 02:48	1.56
...	C	20	2006-01-04 03:02	1.59
...	R	10	2006-01-04 03:04	1.59
...	I	10	2006-01-04 03:07	1.60
mb03	02 ^h 00 ^m	-73° 00'	C	600	2006-01-05 01:16	1.40
...	R	300	2006-01-05 01:42	1.42
...	I	300	2006-01-05 01:57	1.44
...	C	20	2006-01-05 01:40	1.42
...	R	10	2006-01-05 01:55	1.44
...	I	10	2006-01-05 02:10	1.46
mb06	02 ^h 24 ^m	-73° 54'	C	600	2006-01-04 03:47	1.60
...	R	300	2006-01-04 04:13	1.66
...	I	300	2006-01-04 04:28	1.70
...	C	20	2006-01-04 04:11	1.65
...	R	10	2006-01-04 04:26	1.69
...	I	10	2006-01-04 04:42	1.73
mb08	02 ^h 42 ^m	-73° 30'	C	600	2006-01-05 02:13	1.42
...	R	300	2006-01-05 02:38	1.45
...	I	300	2006-01-05 02:53	1.47
...	C	20	2006-01-05 02:36	1.45
...	R	10	2006-01-05 02:51	1.47
...	I	10	2006-01-05 03:07	1.49
mb09	03 ^h 00 ^m	-73° 30'	C	600	2006-01-04 04:43	1.64
...	R	300	2006-01-04 05:09	1.71
...	I	300	2006-01-04 05:24	1.75
...	C	20	2006-01-04 05:07	1.70
...	R	10	2006-01-04 05:22	1.74
...	I	10	2006-01-04 05:38	1.79
mb11	03 ^h 18 ^m	-74° 00'	C	600	2006-01-05 03:11	1.46
...	R	300	2006-01-05 03:37	1.49
...	I	300	2006-01-05 03:52	1.51
...	C	20	2006-01-05 03:35	1.49
...	R	10	2006-01-05 03:50	1.51
...	I	10	2006-01-05 04:06	1.54
mb13	03 ^h 36 ^m	-74° 30'	C	600	2006-01-04 05:52	1.74
...	R	300	2006-01-04 06:17	1.81
...	I	300	2006-01-04 06:33	1.86
...	C	20	2006-01-04 06:15	1.80
...	R	10	2006-01-04 06:31	1.85
...	I	10	2006-01-04 06:46	1.91
mb14	03 ^h 42 ^m	-73° 18'	C	600	2006-01-05 04:20	1.51
...	R	300	2006-01-05 04:45	1.55
...	I	300	2006-01-05 05:00	1.59
...	C	20	2006-01-05 04:43	1.55
...	R	10	2006-01-05 04:58	1.58
...	I	10	2006-01-05 05:14	1.62
mb16	03 ^h 54 ^m	-75° 00'	C	600	2006-01-05 05:17	1.62
...	R	300	2006-01-05 05:42	1.68
...	I	300	2006-01-05 05:57	1.73
...	C	20	2006-01-05 05:40	1.68
...	R	10	2006-01-05 05:56	1.71
...	I	10	2006-01-05 06:18	1.77
mb18	04 ^h 12 ^m	-75° 00'	C	600	2006-01-04 06:48	1.80
...	R	300	2006-01-04 07:14	1.88
...	I	300	2006-01-04 07:29	1.93
...	C	20	2006-01-04 07:12	1.87
...	R	10	2006-01-04 07:27	1.93
...	I	10	2006-01-04 07:42	1.98
mb19	04 ^h 30 ^m	-75° 00'	C	600	2006-01-05 06:32	1.72
...	R	300	2006-01-05 06:57	1.78
...	I	300	2006-01-05 07:13	1.83
...	C	20	2006-01-05 06:55	1.78
...	R	10	2006-01-05 07:11	1.82
...	I	10	2006-01-05 07:26	1.88
mb20	04 ^h 48 ^m	-74° 30'	C	600	2006-01-05 07:28	1.82
...	R	300	2006-01-05 07:54	1.91
...	I	300	2006-01-05 08:09	1.97
...	C	20	2006-01-05 07:52	1.90
...	R	10	2006-01-05 08:07	1.96
...	I	10	2006-01-05 08:22	2.02

TABLE 2
STANDARD FIELD OBSERVATIONS

Field ID	Right ascension	Declination	Filter	t_{exp} [sec]	Observing time	Airmass	$N_{standards}$
SA 92	00 ^h 55 ^m	00° 40'	<i>C</i>	20	2006-01-04 00:53	1.38	5
...	<i>R</i>	10	2006-01-04 00:55	1.38	89
...	<i>I</i>	10	2006-01-04 00:57	1.39	132
SA 92	00 ^h 55 ^m	00° 40'	<i>C</i>	20	2006-01-04 03:13	3.01	6
...	<i>R</i>	10	2006-01-04 03:15	3.08	98
...	<i>I</i>	10	2006-01-04 03:17	3.14	147
SA 101	09 ^h 57 ^m	-00° 20'	<i>C</i>	20	2006-01-04 05:43	1.34	6
...	<i>R</i>	10	2006-01-04 05:45	1.33	51
...	<i>I</i>	10	2006-01-04 05:47	1.33	79
SA 101	09 ^h 57 ^m	-00° 20'	<i>C</i>	20	2006-01-04 07:47	1.15	6
...	<i>R</i>	10	2006-01-04 07:50	1.15	49
...	<i>I</i>	10	2006-01-04 07:51	1.15	82
SA 98	06 ^h 52 ^m	-00° 24'	<i>C</i>	20	2006-01-04 07:55	1.73	15
...	<i>R</i>	10	2006-01-04 07:57	1.75	662
...	<i>I</i>	10	2006-01-04 07:59	1.77	888
NGC 2298	06 ^h 49 ^m	-36° 00'	<i>C</i>	20	2006-01-04 08:02	1.36	...
...	<i>R</i>	10	2006-01-04 08:04	1.37	515
...	<i>I</i>	10	2006-01-04 08:06	1.38	42
SA 92	00 ^h 55 ^m	00° 40'	<i>C</i>	20	2006-01-05 01:01	1.42	7
...	<i>R</i>	10	2006-01-05 01:03	1.43	97
...	<i>I</i>	10	2006-01-05 01:05	1.44	144
SA 101	09 ^h 57 ^m	-00° 20'	<i>C</i>	20	2006-01-05 04:11	1.91	6
...	<i>R</i>	10	2006-01-05 04:13	1.88	55
...	<i>I</i>	10	2006-01-05 04:15	1.86	80
SA 101	09 ^h 57 ^m	-00° 20'	<i>C</i>	20	2006-01-05 06:23	1.22	7
...	<i>R</i>	10	2006-01-05 06:25	1.22	52
...	<i>I</i>	10	2006-01-05 06:27	1.22	77

TABLE 3
PHOTOMETRIC CALIBRATION PARAMETERS

Filter	CCD	Extinction	Ext. Unc.	ZP	ZP Unc.	Color Term	Col. Term Unc.
Night 1							
<i>C</i>	1–8 ^a	0.275	0.0015	0.074	0.0200	-0.100	0.0100
<i>R</i>	1 ^b	0.072	0.0010	-0.690	0.0200	-0.032	0.0130
<i>R</i>	2	0.072	0.0010	-0.706	0.0045	-0.024	0.0077
<i>R</i>	3	0.072	0.0010	-0.684	0.0023	-0.042	0.0039
<i>R</i>	4	0.072	0.0010	-0.670	0.0045	-0.049	0.0083
<i>R</i>	5 ^b	0.072	0.0010	-0.682	0.0200	-0.035	0.0130
<i>R</i>	6	0.072	0.0010	-0.680	0.0033	-0.044	0.0050
<i>R</i>	7	0.072	0.0010	-0.666	0.0027	-0.052	0.0042
<i>R</i>	8	0.072	0.0010	-0.703	0.0027	-0.030	0.0050
<i>I</i>	1	0.040	0.0009	-0.029	0.0185	-0.003	0.0140
<i>I</i>	2	0.040	0.0009	0.009	0.0022	0.007	0.0016
<i>I</i>	3	0.040	0.0009	0.008	0.0020	-0.001	0.0016
<i>I</i>	4	0.040	0.0009	0.014	0.0038	0.005	0.0041
<i>I</i>	5 ^b	0.040	0.0009	-0.006	0.0230	0.003	0.0090
<i>I</i>	6	0.040	0.0009	-0.011	0.0020	0.012	0.0015
<i>I</i>	7	0.040	0.0009	0.010	0.0015	0.003	0.0013
<i>I</i>	8	0.040	0.0009	-0.003	0.0031	0.010	0.0022
Night 2							
<i>C</i>	1–8 ^a	0.299	0.0012	0.026	0.0200	-0.087	0.0100
<i>R</i>	1 ^b	0.090	0.0010	-0.731	0.0200	-0.021	0.0130
<i>R</i>	2	0.090	0.0010	-0.732	0.0078	-0.022	0.0140
<i>R</i>	3	0.090	0.0010	-0.707	0.0030	-0.032	0.0050
<i>R</i>	4	0.090	0.0010	-0.727	0.0088	-0.047	0.0176
<i>R</i>	5 ^b	0.090	0.0010	-0.723	0.0200	-0.024	0.0130
<i>R</i>	6	0.090	0.0010	-0.710	0.0055	-0.030	0.0082
<i>R</i>	7	0.090	0.0010	-0.727	0.0067	-0.022	0.0094
<i>R</i>	8	0.090	0.0010	-0.748	0.0043	-0.020	0.0079
<i>I</i>	1 ^b	0.061	0.0007	-0.038	0.0220	0.007	0.0130
<i>I</i>	2	0.061	0.0007	-0.011	0.0025	0.002	0.0017
<i>I</i>	3	0.061	0.0007	-0.030	0.0047	0.004	0.0038
<i>I</i>	4	0.061	0.0007	-0.003	0.0111	-0.019	0.0109
<i>I</i>	5 ^b	0.061	0.0007	-0.033	0.0200	0.001	0.0130
<i>I</i>	6	0.061	0.0007	-0.029	0.0026	0.018	0.0021
<i>I</i>	7	0.061	0.0007	-0.021	0.0031	-0.002	0.0021
<i>I</i>	8	0.061	0.0007	-0.029	0.0028	0.011	0.0020

^a There were too few *C* standards to support an independent transformation solution for each CCD.

^b There were too few standards in this CCD to support an independent transformation solution. The zeropoint and color term values for this CCD are bootstrapped from the values published at the CTIO website.

TABLE 4
PHOTOMETRY OF STARS IN MAGELLANIC BRIDGE FIELDS

Object ID	Right ascension	Declination	<i>C</i> [mag]	σ_C [mag]	<i>R</i> [mag]	σ_R [mag]	<i>I</i> [mag]	σ_I [mag]
Region mb02								
1	01 ^h 43 ^m 10.7 ^s	-74° 37' 51"	19.187	0.037	19.416	0.028	19.385	0.039
2	01 ^h 43 ^m 10.7 ^s	-74° 38' 52"	21.070	0.087	20.796	0.115
3	01 ^h 43 ^m 10.9 ^s	-74° 37' 36"	18.075	0.037	18.486	0.026	18.482	0.032
4	01 ^h 43 ^m 11.0 ^s	-74° 44' 39"	21.457	0.116	20.501	0.052
5	01 ^h 43 ^m 11.2 ^s	-74° 33' 20"	20.255	0.045	19.720	0.059
6	01 ^h 43 ^m 11.2 ^s	-74° 36' 26"	20.416	0.060	18.901	0.023	18.379	0.033
7	01 ^h 43 ^m 11.2 ^s	-74° 37' 22"	20.728	0.065	19.807	0.041	19.424	0.038
8	01 ^h 43 ^m 11.5 ^s	-74° 36' 02"	19.034	0.030	18.538	0.033
9	01 ^h 43 ^m 11.8 ^s	-74° 48' 51"	21.007	0.071	20.693	0.078
10	01 ^h 43 ^m 11.9 ^s	-74° 45' 31"	17.561	0.035	15.270	0.032

NOTE. — The complete version of this table is in the electronic edition of the Journal. The printed edition contains only a sample.

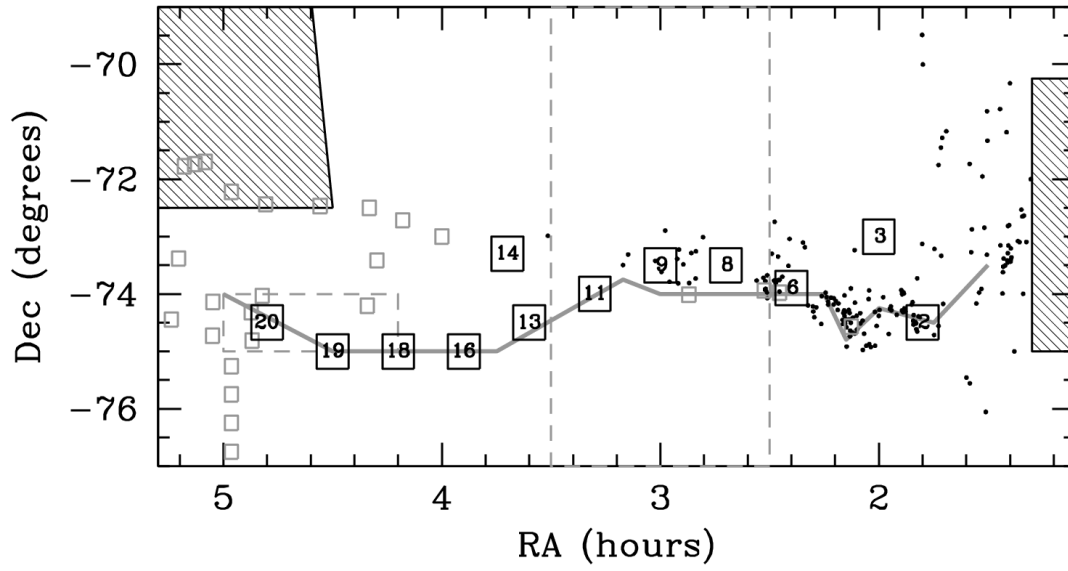


FIG. 1.— A schematic view of the Magellanic Bridge region. The positions of the twelve observed CTIO-4m fields are shown as numbered boxes. The inter-Cloud fields previously observed by Demers & Battinelli (1998) are shown as gray boxes. Star clusters from Bica & Schmitt (1995) are shown as points. The gray line is an approximate trace of the HI ridgeline through the inter-Cloud region, from Figure 1 in Putman (2000). The hashed areas represent the portions of the regions covered by the Magellanic Clouds Photometric Survey (LMC at left, Zaritsky et al. 2004; SMC at right, Zaritsky et al. 2002).

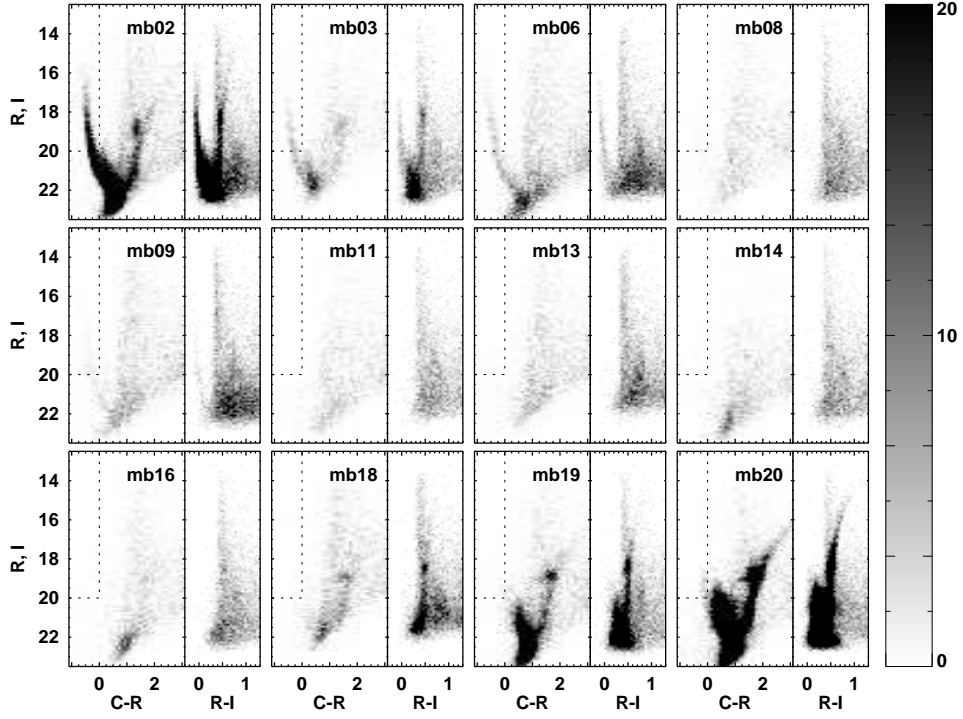


FIG. 2.— Color-magnitude Hess diagrams of each of the twelve fields observed in the Magellanic Bridge. Each pair of panels consists of the $C - R, R$ CMD (left) and the $R - I, I$ CMD (right). The fields are numbered in order of increasing right ascension (see Figure 1). Dashed lines indicate the region of the $C - R$ CMDs where main sequence stars younger than 1 Gyr are expected. The pixel values indicate the number of stars present in each pixel, ranging from zero (white) to 20 (black), as indicated by the scale bar on the right.

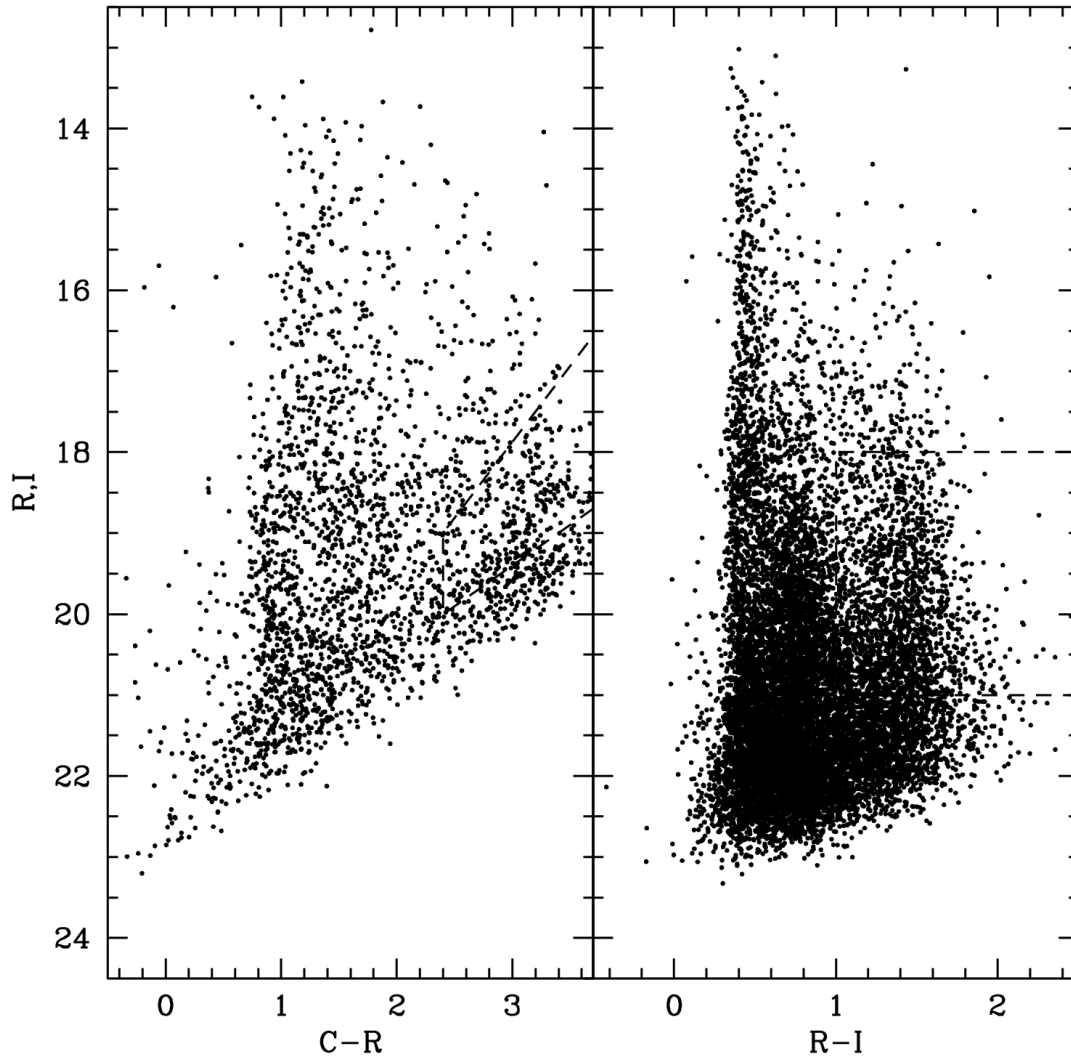


FIG. 3.— The CMD pair for the offset field, which has a similar Galactic latitude to the Bridge fields, but lies to the west of the SMC. It therefore should represent a pure foreground Galactic and background extragalactic population. As in Figure 2, the $C - R, R$ CMD is shown at left, and the $R - I, I$ CMD is shown at right. The normalization regions, which are expected to contain only contaminant objects, are outlined with dashed lines.

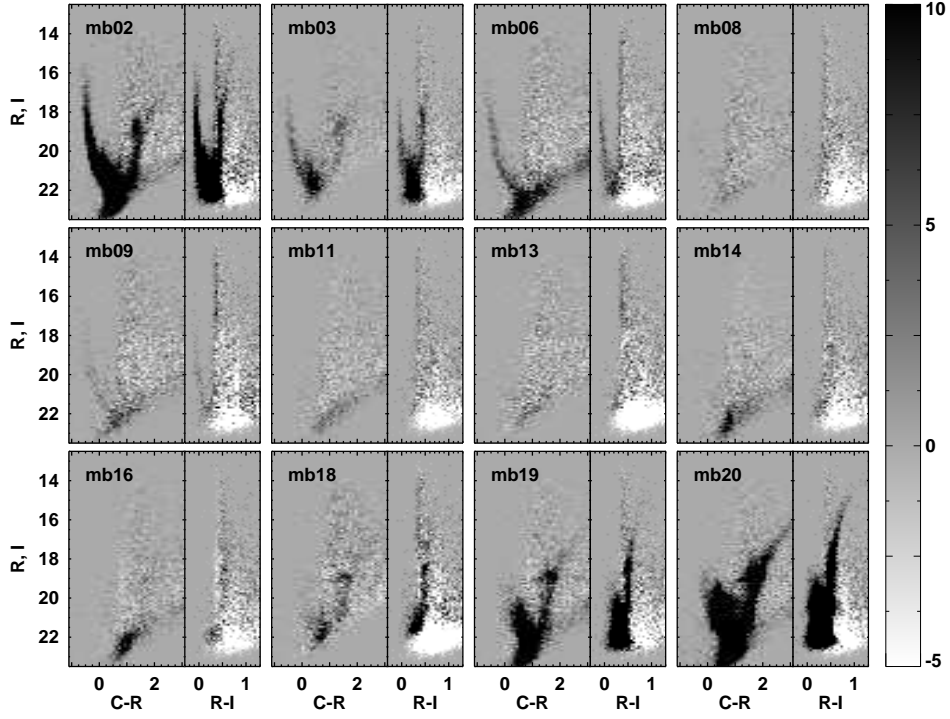


FIG. 4.— Color-magnitude Hess diagrams of the twelve observed Bridge fields, after statistically subtracting a contaminant component derived from the offset field population (see Figure 3). Darker pixels indicate a local excess of stars compared to the contaminant population, whereas lighter pixels indicate a local deficit of stars. In a perfect subtraction, the pixels lighter than the medium gray of zero difference would be consistent with the noise of the subtraction. Many of the fields show large deficits of stars at the faint end of the $R-I$ CMD; we believe this is due to a mismatch in the faint limit between these target fields and the offset field. The pixel values indicate the difference in star counts ($N_{field} - N_{offset}$) for each pixel, ranging from -5 (white) to +10 (black), as indicated by the scale bar on the right.

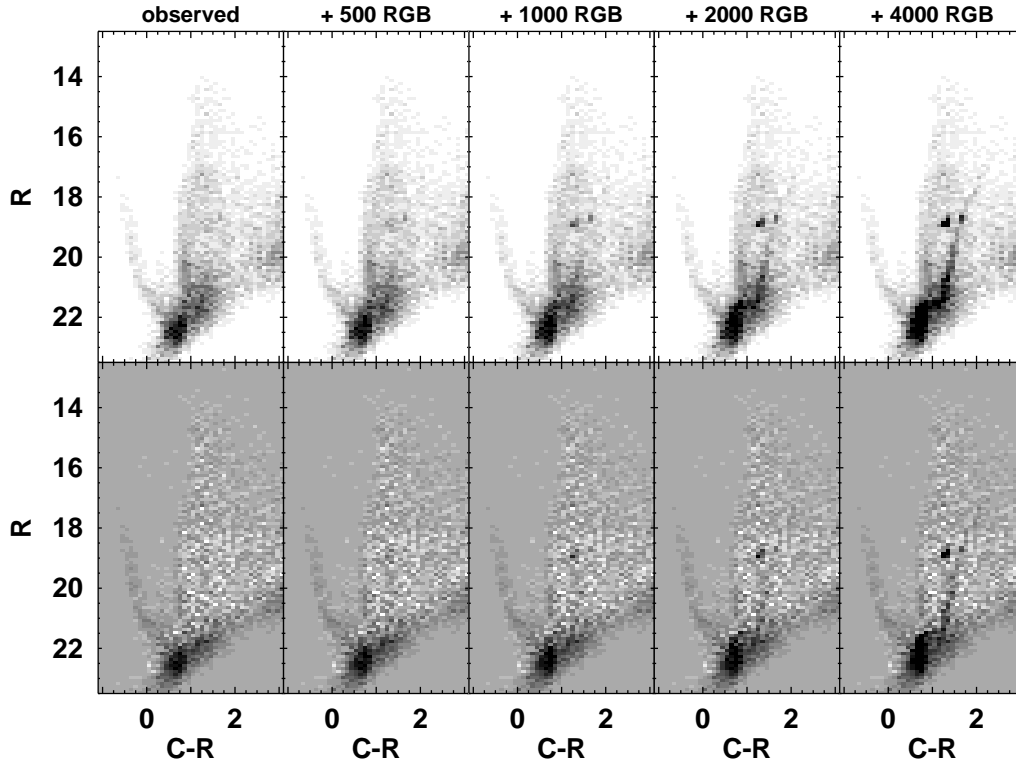


FIG. 5.— The top left panel shows the $C - R$ Hess diagram for a composite population formed by combining the “true Bridge” fields (mb06–mb14). We see no trace of a red giant branch feature which would indicate an older stellar population in these fields. We determine the upper limit on the number of red giants which could remain undetected in this diagram by adding a synthetic red giant branch composed of increasing numbers of stars. From left to right, starting with the second panel we show the same Hess diagram after having added 500, 1000, 2000, and 4000 synthetic red giant stars. The bottom row of panels show the same Hess diagrams, after having statistically subtracted a contaminant population derived from the offset field.

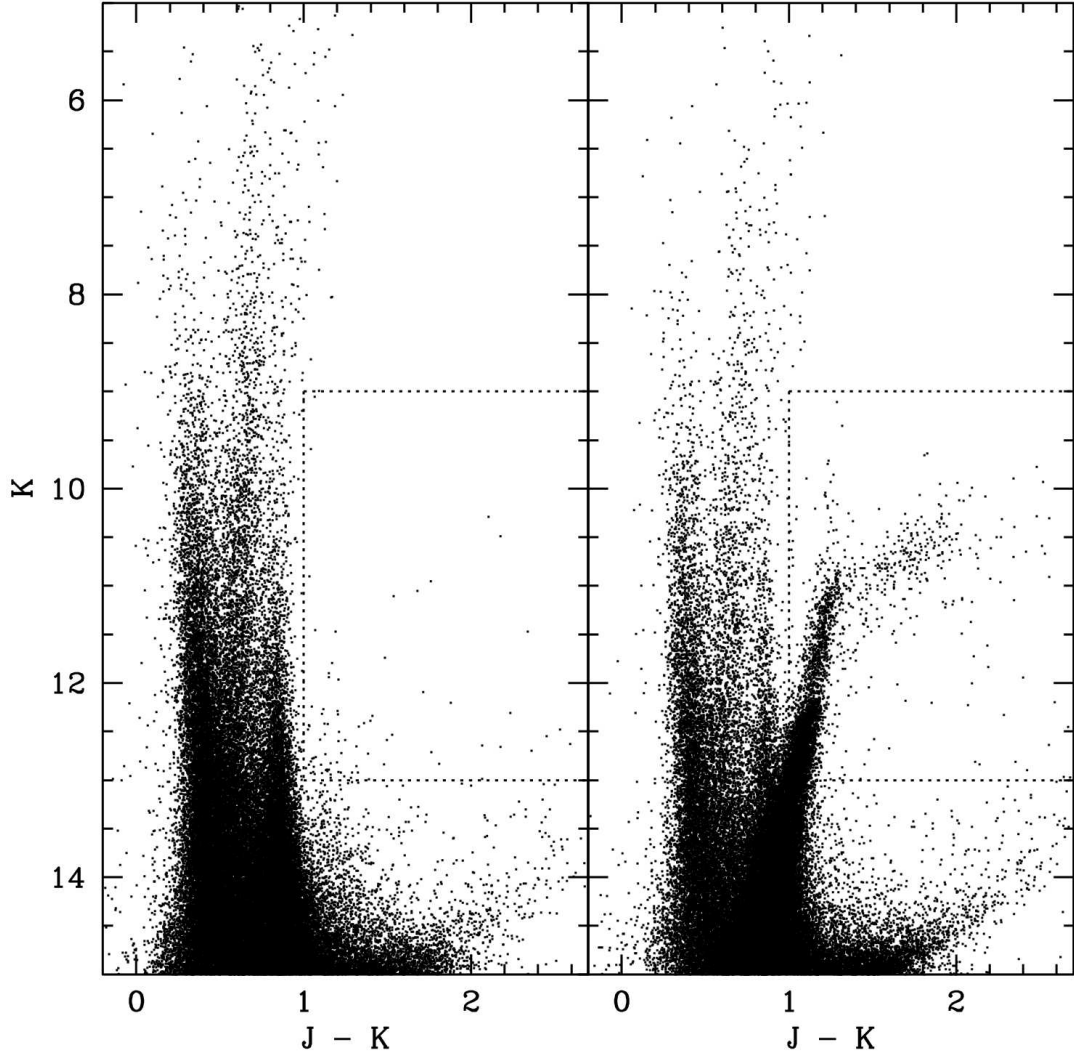


FIG. 6.— Near-infrared $J-K$ color-magnitude diagrams for two regions between the Magellanic Clouds. At left is the “full-bridge region”, which spans 35 square degrees and is designed to cover the full region between the Clouds that is not contaminated by stars bound to either galaxy. At right is the “SW-LMC region”, which covers 3.2 square degrees and is coincident with our fields mb18, mb19, and mb20, in which we have observed an old stellar population associated with the LMC. The dotted lines in each panel indicate the region where the bright red giant and asymptotic giant branches are expected at the distance of the Magellanic system. While an abundant population of these stars is present in the SW-LMC region, the much larger full-bridge region contains hardly any such stars.

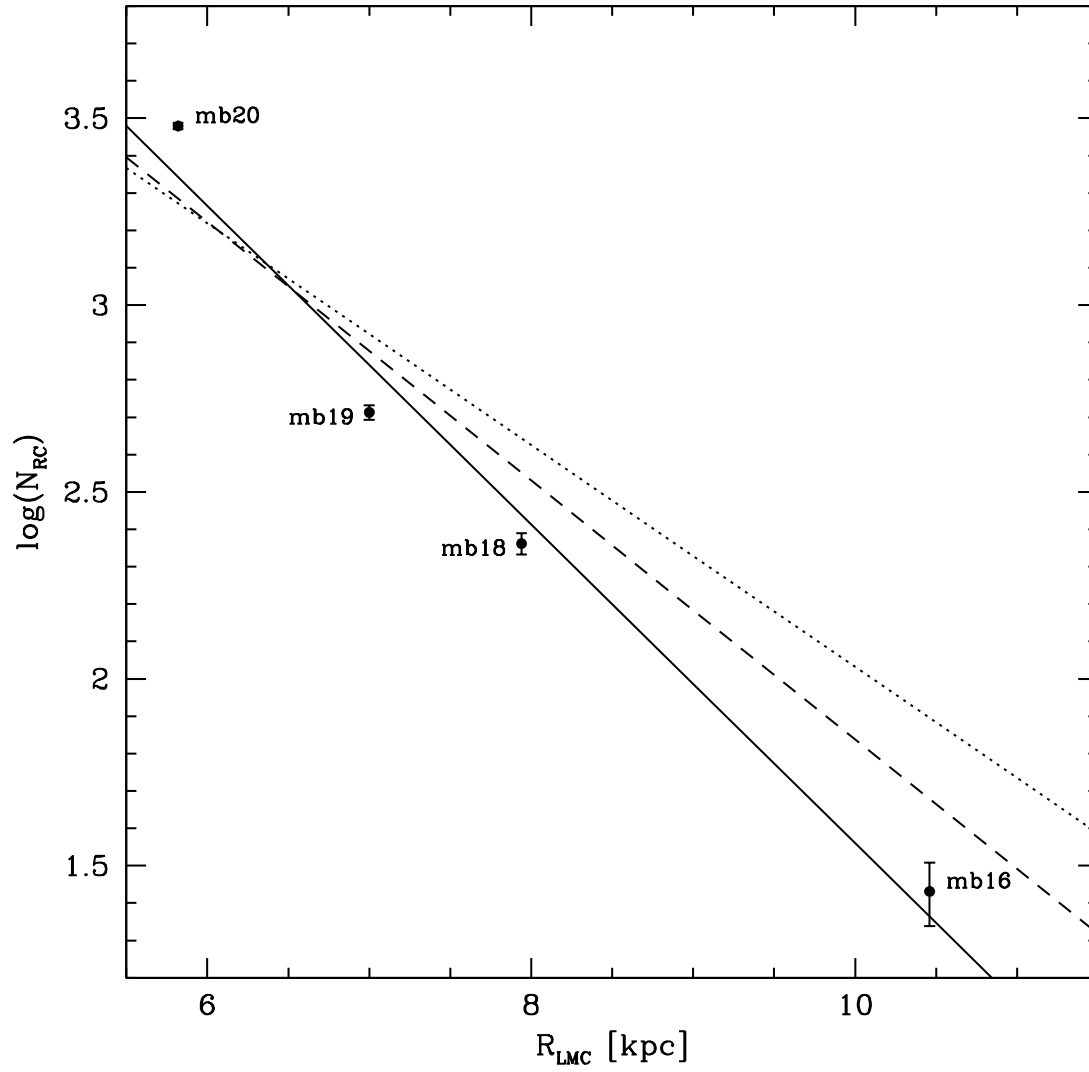


FIG. 7.— The number of red clump stars present in fields mb16–mb20 vs. the physical distance of each field from the center of the LMC. In determining these distances, we have assumed that the red clump stars are in the disk of the LMC, whose geometry is known. The best-fit exponential-disk model for these data is shown as the solid line, and it is similar to previous determinations of the LMC’s exponential disk by (Hardy 1978, ; dashed line) and (Gallart et al. 2004, ; dotted line).

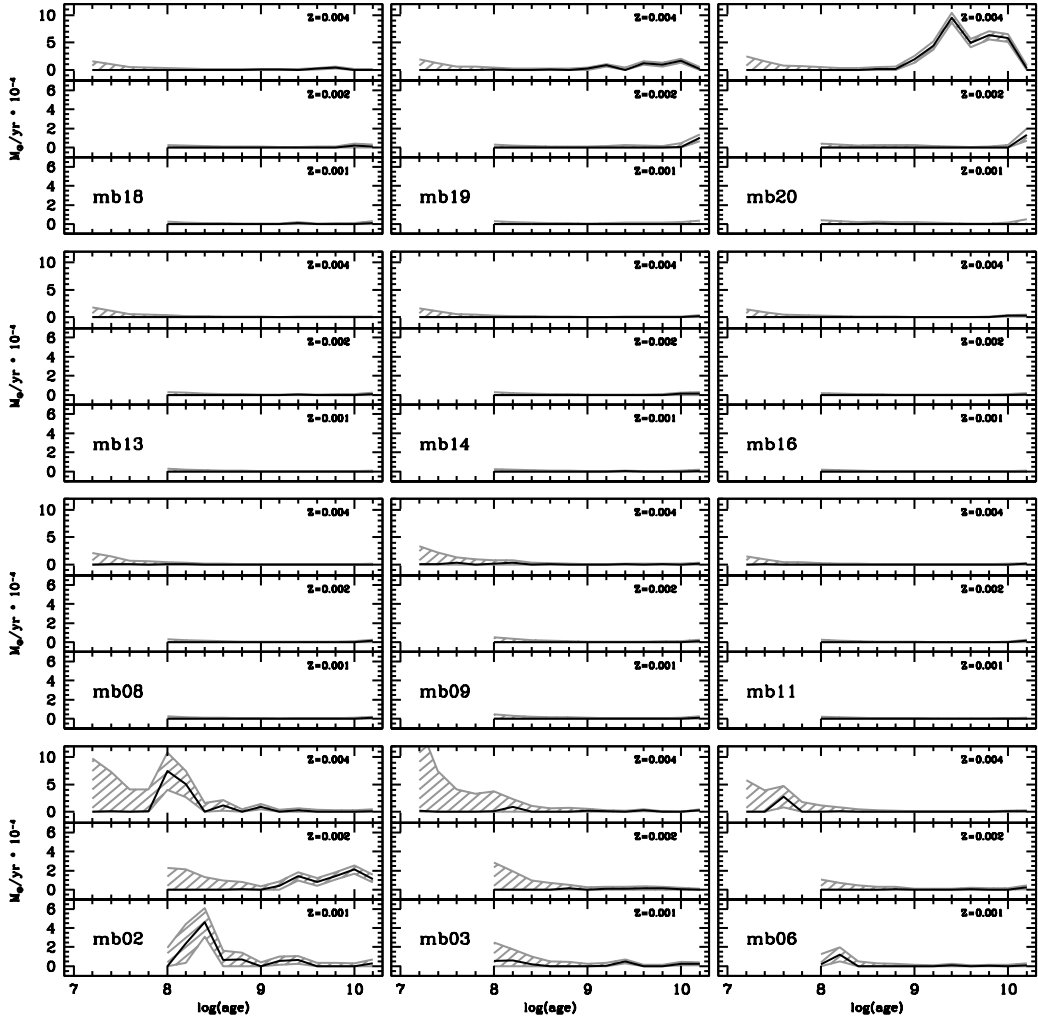


FIG. 8.— StarFISH SFH solutions for the twelve observed fields in the Magellanic Bridge. Each panel is divided into three subpanels, showing the star formation rate as a function of time for three metallicities (top to bottom: $Z=0.004$, $Z=0.002$, and $Z=0.001$). The best-fit history is plotted with a heavy line in each sub-panel, and the shaded gray regions indicate the estimated uncertainty of the solution. Fields are presented in order of increasing right ascension, starting with mb02 (the field nearest the SMC) in the lower left, up to mb20 (the field nearest the LMC) in the upper right.

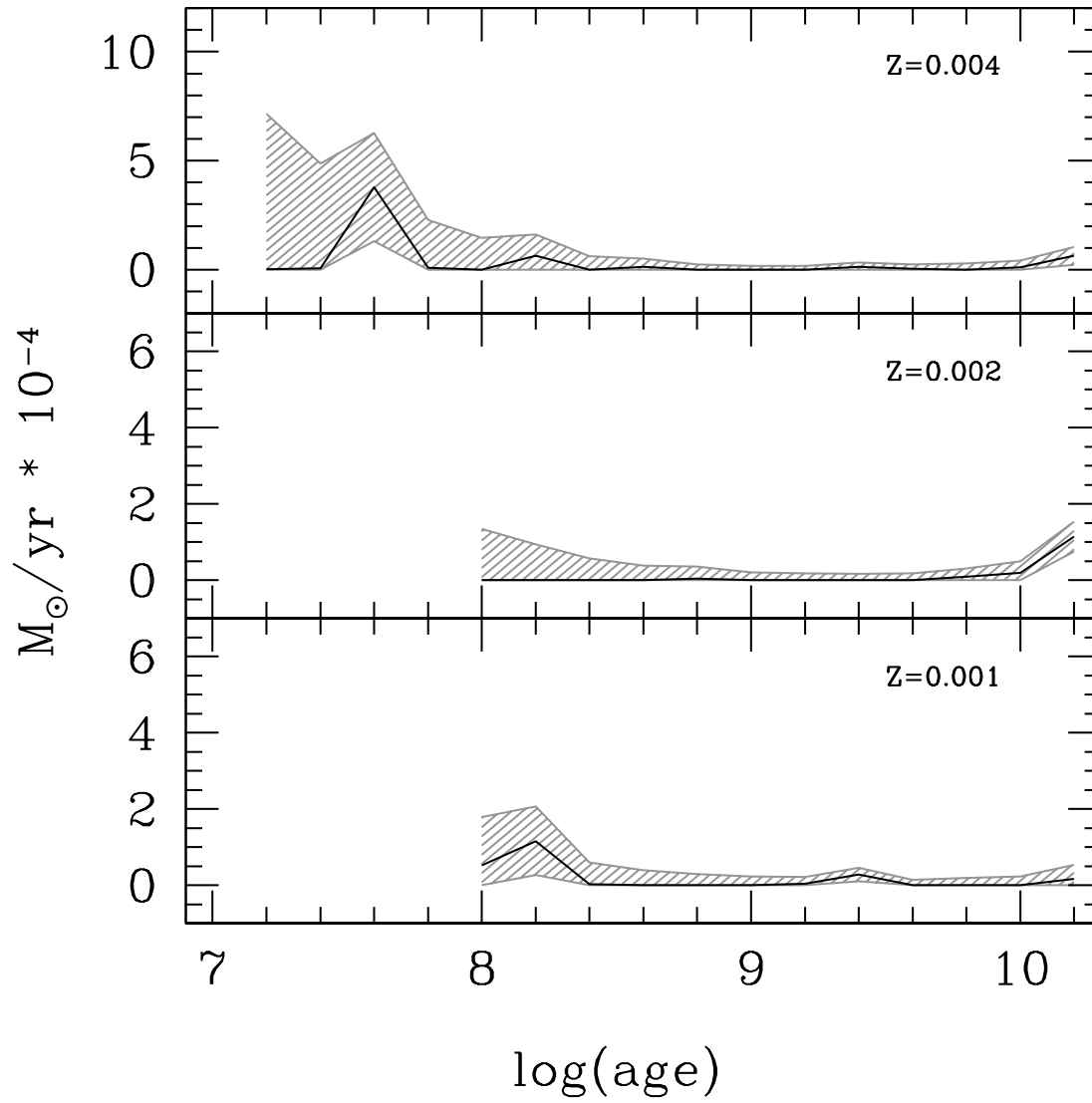


FIG. 9.— The SFH solution for a composite population formed from fields mb06–mb09. The solutions for these fields presented in Figure 8 are inconclusive, due to the small number of stars in these fields. By forming a composite population, we can better constrain the average history of these three regions.